Sensors and Actuators B 242 (2017) 1142–1154

Contents lists available at ScienceDirect

Sensors and Actuators B: Chemical

journal homepage: www.elsevier.com/locate/snb

Substrate-gate coupling in ZnO-FET biosensor for cardiac troponin I detection

M.F.M. Fathil[a], M.K. Md Arshad[a,b,*], A.R. Ruslinda[a], Subash C.B. Gopinath[a,c], M. Nuzaihan M.N.[a], R. Adzhri[a], U. Hashim[a,b], H.Y. Lam[d]

[a] Institute of Nano Electronic Engineering (INEE), Universiti Malaysia Perlis (UniMAP), 01000 Kangar, Perlis, Malaysia
[b] School of Microelectronic Engineering, Universiti Malaysia Perlis (UniMAP), 02600 Arau, Perlis, Malaysia
[c] School of Bioprocess Engineering, Universiti Malaysia Perlis (UniMAP), 02600 Arau, Perlis, Malaysia
[d] Clinical Research Centre (CRC), Hospital Pulau Pinang, 10990 Georgetown, Pulau Pinang, Malaysia

ARTICLE INFO

Article history:
Received 30 June 2016
Received in revised form
19 September 2016
Accepted 21 September 2016
Available online 22 September 2016

Keywords:
Biosensor
Electrical-based
Field-effect transistor
Zinc oxide nanoparticles
Substrate-gate coupling
Cardiac troponin I

ABSTRACT

Currently, field-effect transistor (FET)-based biosensors have been implemented in several portable sensors with the ultimate application in point-of-care testing (POCT). In this paper, we have designed substrate-gate coupling in FET-based biosensor for the detection of cardiac troponin I (cTnI) biomarker. In the device structure, zinc oxide nanoparticles (ZnO-NPs) thin film were deposited through sol-gel and spin coating techniques on the channel. The p-type silicon was used as a substrate, while ZnO is an n-type nanomaterial, thus creates *p-n*-p junction between source, channel, and drain. The deposited thin films exhibited hexagonal wurtzite phase of ZnO, suitable for biomolecular interaction as revealed in X-ray diffraction (XRD) analysis. The surface of the thin film was then functionalized with 3-aminopropyltriethoxysilane (APTES), followed by glutaraldehyde (GA) as a bi-functional linker to immobilize the cTnI monoclonal antibody (MAb-cTnI) as bio-receptor for capturing cTnI biomarker and proven by the Fourier transform-infrared (FT-IR) spectra. Lastly, we demonstrated a new strategy, the integration of FET-based biosensors with substrate-gate showed differences between before (immobilization) and after cTnI target biomarker interaction by significant changes in drain current (I_D) and change of threshold voltage (V_T), which improved the sensitive detection, with the limit of detection down to 3.24 pg/ml.

1. Introduction

Field-effect transistor (FET)-based biosensors are currently at the centre of interest for biological molecules (biomolecules) detection due to anticipated qualities, i.e., label-free, fast electrical detection, low power operation, easy to move from one place to another, low cost for mass production, and both sensor and measurement system are compatible to be integrated into a single chip [1]. The working principle of the FET-based biosensor that enables the detection of biomolecules is based on the production of difference surface potential on the surface of a transducer upon biological interaction, thus contribute to modulation of the current flow inside the channel, located between two regions, which are drain and source [2]. The specific detection of biomolecules is possible by utilizing specific biological receptors (bio-receptors), i.e., DNA, RNA, aptamers, or antibodies, which are immobilize at the surface of the transducer through covalent binding with suitable chemical linkers. The biomolecules, which can be positively or negatively charge, captured by the bio-receptors, influence the changes in electrical behaviour of the transducers, whether increase or decrease (depending on the n- or p-type of semiconductor materials) the conductance of the transducer's channel [1], allowing more or less current flows from source to drain region. Several gating approaches on FET-based biosensor have been demonstrated in the literature [3–9], which are possible to enhance their performance in biomolecules detection with higher sensitivity. Lee et al. [6] and Nuzaihan et al. [9] utilized a single liquid and molecular gate control, respectively, where modulation of surface charge through the nanowires (gate) occurred during interaction between bio-receptor and target molecule, thus influences the conductivity of

* Corresponding author at: Institute of Nano Electronic Engineering (INEE), Universiti Malaysia Perlis (UniMAP), 01000 Kangar, Perlis, Malaysia.
E-mail addresses: faris.fathil@gmail.com (M.F.M. Fathil), mohd.khairuddin@unimap.edu.my (M.K. Md Arshad), ruslinda@unimap.edu.my (A.R. Ruslinda), subash@unimap.edu.my (S.C.B. Gopinath), m.nuzaihan@unimap.edu.my (M. Nuzaihan M.N.), adzhri@gmail.com (R. Adzhri), uda@unimap.edu.my (U. Hashim), drlamhy@yahoo.ca (H.Y. Lam).

http://dx.doi.org/10.1016/j.snb.2016.09.131
0925-4005/

the nanowires. The deployment of single gate also was reported by Iskierko et al. [5], but with enhancement through introduction as an extended-gate, whereby the functionalized gate is extended from the FET, hence separated the FET from the chemical environment. In addition, different device architecture was presented by Ahn et al. [10], a double-gate nanowire FET, where the sensitivity is improved by controlling the conduction channel in the silicon nanowire through the application of bias symmetric/asymmetric on double-gate, which are located at both sides of the nanowire. Different approach or device architecture of double gate FET [3,4,8,11] was presented utilizing the back-gate, which provides low threshold voltage (V_T) values, suggests a more effective back-gate coupling.

Determination of a suitable transducer's material for the FET-based biosensor is also another crucial criterion, which need to be considered properly. Nanomaterials offer high surface area for higher biomolecules loading and help biomolecules to maintain its bioactivity by providing a suitable microenvironment [12]. They also enable direct electron transfer between the biomolecule's active site and electrode [13]. Zinc oxide (ZnO) is an example of II–IV metal-oxide semiconductor nanomaterials with wide band gap (3.37 eV) have attracted many researchers due to its broad range of applications [14,15]. Its high isoelectric point (9.5) trigger a distinct property to immobilize biomolecules having a low isoelectric point through electrostatic interaction, in addition to biocompatibility and abundance in nature have captured researchers' attention as a transducer in biosensors. ZnO is a favourable material for immobilization of biomolecules and can be utilized for biosensor development due to non-toxicity, high chemical stability, and high electron transfer capability [16], thus improved bio-sensing characteristics. In the recent years, several FET-based studies have adapted different ZnO nanostructures as transducer in their device for bio-sensing applications [17]. An enzyme-coated single ZnO nanowire FET-biosensor fabricated by electron-beam lithography by Liu et al. [18] capable of detecting uric acid with limit of detection down to 1 pM. Another study by Ogata et al. [19] utilized hydrothermally-grown ZnO nanorods integrated with FET-based biosensor demonstrated a detection limit of ~50 nM.

Proper preparation of ZnO nanoparticles (ZnO-NPs) seed solution and deposition method via spin coating technique are important to produce uniform ZnO-NPs thin film as a transducer for biosensor. Sol-gel approach is an attractive process in thin film fabrication because of its inexpensive, low temperature process, and can be scattered uniformly on the substrate. Further, sol–gel technique requires small quantities of precursor material for preparation, possible to synthesis materials that are high volatilization and high melting temperature, high purity process resulting high homogeneity and possible to produce various form of structures. The preparation process is crucial to ensure the ZnO-NPs seed solution from sol-gel technique can be deposited and becomes ZnO-NPs thin film on the SiO_2 layer. Further, the existence of the ZnO thin film, structure, and its electrical characteristic needed to be verified in order to use it as a sensing element for the FET-based biosensors.

In this paper, we combined the benefit of having substrate-gate coupled with n-type ZnO-NPs thin film deposited at a micro-sized channel in between of p-type silicon layer on a silicon-on-insulator (SOI) wafer, via low cost sol-gel and spin coating technique to form an *p-n-*p junction ZnO-FET biosensor for the detection of cardiac troponin I (cTnI) biomarker. The introduction of *p-n-*p junction in the FET-based biosensor is an alternate approach for the electrical label-free detection, which 1) simplify the fabrication process compared to three-dimensional (3D) device architecture, i.e., nanowires and 2) the channel at the *p-n-*p junction can be controlled/influenced by the gate, i.e., substrate-gate (thus ambipolar conduction can be achieved, either hole or electron conduction depending on substrate-gate bias) and charge from the biomolecules at the channel area. The main reasons for ZnO-NPs thin film selection as channel/transducer for the FET biosensor was due to 1) biocompatible material, 2) n-type material, which can be integrated with p-type silicon to form *p-n-*p junction, 3) simple and inexpensive deposition method, and 4) high surface area can be accomplished with deposition of nanoparticle for biomolecules capturing. A device modelling simulation was performed in order to understand the electrical behaviour of our biosensor. Next, the biosensor was fabricated through conventional lithography processes, which requires less complexity in fabrication of the device, compared to 3D nanowires. Thus, the need of sophisticated nanoscale fabrication process can be eliminated. For example, fabrication of a double-gate nanowire FET for biosensing requires 193 nm wavelength lithography equipment [10]. In our approach, sol-gel technique produces high uniformity ZnO-NPs thin film from a formation of dense nanoparticles at low cost. Several characterizations of produced thin film were performed based on the surface morphology, structure, crystalline phase, and electrical properties for further investigation. The surface of the thin film was chemically modified to enable immobilization of cTnI monoclonal antibody (MAb-cTnI) as bio-receptor for capturing specific cTnI biomarker. The completed device was demonstrated for the performance in detection of various concentration of positively charged cTnI biomarker with isoelectric point (pI) of 9.87 [20] at the sensing area in dry condition (Fig. 1). At this stage, we combined the FET-based biosensor with the voltage biasing from the substrate of the SOI wafer (with silicon body thickness of 70 nm and buried oxide (BOX) thickness of 145 nm), thus producing substrate-gate coupling, where the detection sensitivity is expected to be improved by controlling the conduction channel and allowing more I_D across the channel in the ZnO-NPs thin film between the p-type source and drain region.

2. Materials and methods

2.1. Preparation of wafers

A p-type (8.5-22.5 ohm·cm) SOI (Soitec, Grenoble, France) wafer with thickness of 70 nm and 145 nm for top-silicon and BOX layer, respectively, was used in this work. The wafer was cleaned by using RCA1 and RCA2 standard solutions at 60 °C for 10 min to eliminate organic and inorganic contaminants on its surface, respectively. Each processes were followed by rinsing with deionized (DI) water thoroughly.

2.2. Preparation of ZnO nanoparticles seed solution

In this work, zinc acetate dihydrate ($Zn(CH_3COO)_2{\cdot}2H_2O$) (ACS reagent; Sigma Aldrich, St. Louis, Missouri, USA) powder as a precursor, was mixed with 100 ml of 2-propanol ($CH_3CHOHCH_3$) (U.S.P; J.T. Baker, Centre Valley, Pennsylvania, USA) inside a volumetric flask. The molar concentration of $Zn(CH_3COO)_2{\cdot}2H_2O$ was kept at 200 mM. The mixed solution was vigorously stirred at 1000 rpm by using magnetic stirrer with hotplate (MSH-30D; WiseStir®, Wertheim, Germany) at 60 °C for 20 min. The solution changed its color into milky white, signified $Zn(CH_3COO)_2{\cdot}2H_2O$ had dissolved properly inside $CH_3CHOHCH_3$. The stirred solution was then added drop wise with ethanolamine (C_2H_7NO) (purified by redistillation, ≥99.5%; Sigma-Aldrich, St. Louis, Missouri, USA) by 10 min interval between each drop, while continuously stirred for the next 120 min until a homogenous and transparent solution was produced. The molar ratio between $Zn(CH_3COO)_2{\cdot}2H_2O$ and C_2H_7NO was precisely maintained at 1. Finally, the seed solution was left to age at room temperature for 24 h.

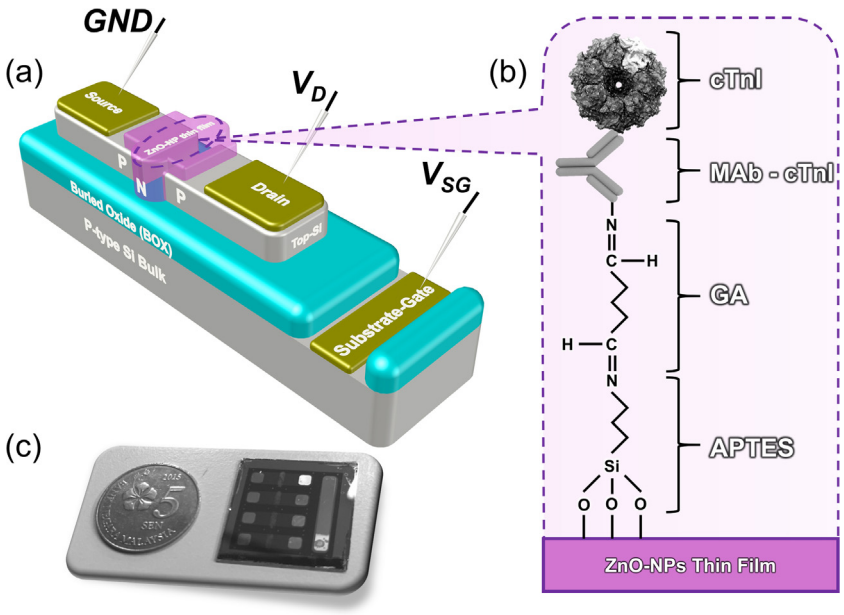

Fig. 1. Electrical detection of cTnI biomarker by ZnO-FET biosensor with substrate-gate coupling. (a) The 3D representation of the biosensor. (b) The surface functionalization of ZnO-NPs thin film with 3-aminopropyltriethoxysilane and glutaraldehyde; followed by surface immobilization process with cTnI monoclonal antibody for capturing cTnI biomarker. (c) The fabricated biosensor, comparable in size with Malaysia's 5 cent.

2.3. Fabrication of substrate-gate coupling with ZnO-FET biosensor

The device fabrication was performed by using the cleaned SOI wafer, which was prepared previously. The source and drain of the FET were obtained through conventional lithography process on the top silicon layer. The lithography process was started by spin coating of positive photoresist (PR1-2000A; Futurrex, Franklin, New Jersey, USA) on the SOI wafer via spin coater at 3000 rpm for 40 s, producing resist thickness approximately 1.8 μm. The resist was then soft-baked at 110 °C for 90 s on hot plate to improve photoresist adhesion to the wafer, prior source and drain patterns transfer process via UV light exposure with wavelength of 365 nm for 10 s inside a mask aligner (MDA–400 M; Midas System, Daejeon, Korea). The patterns were then developed by using resist developer (RD6; Futurrex, Franklin, New Jersey, USA) until source and drain pattern transferred on the top-silicon layer after approximately ~35 s and rinsed with DI water. To decrease removability of the stabilized resist after processing, the wafer was hard-bake at 110 °C for 120 s. The source and drain at the top-silicon layer was produced by etching a ~10 μm width channel in between them via inductive couple plasma reactive ion etching (ICP-RIE) (RIE-10iP; Samco, Kyoto, Japan) for 27 s. The remaining photoresist was stripped completely by using C_3H_6O (ACS reagent; R & M chemicals, Edmonton, Alberta, Canada) and rinsed by using DI water. The process continued with substrate-gate exposure, which was also went through similar conventional lithography process as previously stated. However, the etching process of unwanted BOX layer was conducted by using buffered oxide etch (BOE 10:1; J.T. Baker, Centre Valley, Pennsylvania, USA) for 148 s, followed by rinsing with DI water to expose the bottom silicon layer of the SOI wafer. Before the thin film deposition process, C_3H_6O and $CH_3CHOHCH_3$ were used to clean the wafers inside an ultrasonic bath for 20 min, followed by cleaning with DI water. The deposition of ZnO seed solution on the cleaned wafers were conducted via a spin coater (WS-650MZ-23NPP; Laurell Technologies Corporation, North Wales, Pennsylvania, USA) at spin rate of 3000 rpm for 40s. Afterward, the deposited wafers were baked on magnetic stirrer with hotplate at 60 °C for 10 min, before ramped up to 150 °C for additional 10 min, and self-ramped down to 50 °C. This process helped in reduction of thermal shock effect, which may cause damage or cracking to the thin film. In addition, it improved the adhesion between ZnO-NPs thin film with the SOI wafer. The deposition processes were repeated in order to produce three different number of ZnO-NPs thin film deposited layers (1, 3, and 5 coating), thus enable a study of their effects on thin films' surface morphology, structural and crystalline phase, and electrical conductivity. Finally, the coated thin film was annealed at 500 °C for 120 min inside a muffle furnace (OXY2-4-10T; Nanjing Oxy Technology & Trading, Jiangsu Province, China) to produce a ZnO-NPs thin film with hexagonal wurtzite structure, and was let to cool down to room temperature for 1 d. Another lithography process was performed to pattern the thin film as transducer between source and drain area of the FET. The unwanted transducer area was wet-etched by using diluted hydrochloric acid [36.5-38.0%; J.T. Baker, Centre Valley, Pennsylvania, USA in DI water at 1:900 ratios. The photoresist was not stripped in order to protect the thin film from the process ahead. Aluminium thin film was next deposited on the wafer via thermal evaporator (Auto 306; Edwards, Crawley, England), followed by lithography process and etching with aluminium etch (16-1-1-2; J.T. Baker, Centre Valley, Pennsylvania, USA) at 25 °C for 150 s. The remaining photoresist layer was stripped to expose the source, drain, substrate-gate electrodes, and the transducer of the device.

2.4. ZnO-NPs thin film characterization

The characterizations of ZnO-NPs thin film were performed to study the surface morphology, structure, and crystalline phase of the thin film. The surface morphology of the thin films was characterized by using atomic force microscope (AFM) (SPA400; Seiko Instruments Inc., Chiba, Chiba Prefecture, Japan), stylus profilometer (Dektak XT; Bruker, Billerica, Massachusetts, USA) and field-emission scanning electron microscope (FESEM) (NOVA NanoSEM 450; FEI, Hillsboro, Oragon, US), while structural and crystalline phase was analysed by utilizing X-ray diffraction (XRD) (D2 Phaser; Bruker, Billerica, Massachusetts, USA). A semiconductor parametric analyser (SPA) (Keithley 4200-SCS SPA; Keithley

Instruments, Cleveland, Ohio, USA) was used for the electrical measurement of the thin film conductivity.

2.5. Surface functionalization of transducer and characterization

The fabricated device was cleaned by using DI water, $CH_3CHOHCH_3$ and dried for 5 min to promote the surface of transducer with hydroxyl (−OH) group, which already available on the ZnO-NPs thin film [21]. The surface functionalization process is similarly to demonstrated in [22–24]. The process was followed with functionalization transducer by submerging the device into 2% of 3-aminopropyltriethoxysilane (APTES 99%, Sigma-Aldrich, St. Louis, Missouri, USA) in DI water [22] at 25 °C for 120 min and rinsed with DI water for 3 times to remove the unbound APTES residues [23]. The amine-terminated surface was the covalently bound with a bi-functional linker, 2.5% glutaraldehyde (GA) (50% GA in H_20; Sigma-aldrich, St. Louis, Missouri, USA) in DI water at 25 °C for 60 min, to introduce the aldehyde group on the transducer's surface, followed by thorough washing with DI water for 3 times [23]. 10 μg/ml of MAb-cTnI (Mouse monoclonal (3C7) to cTnI; Abcam®, Cambridge, Massachusetts, USA) in 10 mM phosphate buffer solution (PBS 1.0 M, pH 7.4; Sigma-aldrich, St. Louis, Missouri, USA) was applied on the transducer's surface at 25 °C for 120 min for antibody immobilization, continued by completely cleaning with the same buffer for 3 times [24]. The unbound aldehyde groups on the thin film surface were washed and the free surface was blocked by employing 100 mM ethanolamine in PBS at 25 °C for 60 min, followed by cleaning with the same buffer for 3 times [23]. The functional group appeared on the surface of the transducer of the device was examined by using Fourier transform-infrared (FT-IR) spectroscopy (Spectrum 400 FT-IR; PerkinElmer, Utah, USA) after functionalization with APTES, GA, and MAb-cTnI.

2.6. Device modelling of FET-based biosensor

The 2-dimension (2D) cross-sectional structure of the biosensor was designed and simulated by using device modelling simulation software, Silvaco ATLAS to characterize the device electrically when biased with various substrate-gate voltage (V_{SG}). The n-type ZnO-NPs thin film at the channel was doped with concentration of 10^{15} cm^{-3}, while the source and drain region were doped with p-type with concentration of 10^{15} cm^{-3}, thus demonstrating a FET-biosensor with *p-n*-p junction, between source, channel and drain respectively. Demonstration of extra charges i.e positive and negative charges (assumption with values of 6^{10} cm^{-2} and -6^{10} cm^{-2}, respectively), act as charged biomolecules bound on the ZnO-NPs thin film was set in order to observe their effect on threshold voltage (V_T) and drain current (I_D). The simulation was also presented electron concentration versus x-coordinates graphs at horizontal cut near the buried oxide (BOX)/substrate interface and the *p-n*-p junction of the source, channel, and drain, in order to explained the electrical behaviour exhibited by the device during different bias of V_{SG}.

2.7. Electrical characterization of FET-based biosensor

The Keithley 4200-SCS SPA was again used as a three-probe system in the electrical characterization of the biosensor, wherein the drain electrode of the device was supplied by a sweep drain voltage (V_D) from 0 to 5 V, the source electrode was attached to ground, and the substrate-gate electrode was supplied by V_{SG} bias. Based on the setup parameter, the I_D-V_D graph of the initial device without surface functionalization, after surface immobilization with MAb-cTnI and different concentration of cTnI biomarkers were plotted. For cTnI biomarker detection experiment of the devices, 1 μl of various cTnI biomarker concentration (1 ng/ml, 10 ng/ml, 100 ng/ml, 1 μg/ml, and 10 μg/ml) (human cTnI full length protein (ab50803); Abcam®, Cambridge, Massachusetts, USA) in 10 mM PBS was dropped on the functionalized transducer's surface at room temperature for 10 min to allow cTnI binding with the MAb-cTnI, which was previously immobilized [25], continued by completely washing with the same PBS buffer for 3 times thoroughly, to remove any unbound cTnI biomarkers at the surface of the transducer [25]. A negative control experiment was also performed by dropping 1 μl of 10 μg/ml cardiac troponin T (cTnT) (human cTnT protein fragment (AB86685); Abcam®, Cambridge, Massachusetts, USA) in 10 mM PBS on the functionalized transducer's surface at room temperature for 10 min, and again thoroughly washed with the same buffer for 3 times, and blow until dried. For the different concentration detection experiment, the V_D was sweep from 0 to 1 V with step voltage of 0.1 V, while V_{SG} = −2 V was chosen as biased, allowing more current flow at low V_T, which will be discussed later. Electrical measurement was performed for comparison with detection of cTnI biomarker. All electrical measurements for the detection of the cTnI were performed after the device completely dried, without any PBS solution, as reported in [25], to eliminate the occurrence of non-specific adsorption, hence only captured cTnI biomarker by the MAb-cTnI immobilized on the surface of the transducer for characterization.

3. Results and discussions

A FET-based biosensor integrated with ZnO-NPs thin film coupled with substrate-gate was fabricated on SOI wafer through conventional photolithography process. The different deposited layers of the thin films (after annealing process) had produced different in surface topography, desired structural, crystalline phase, and electrical conductivity, for the use as a transducer of the FET-based biosensor. The substrate-gate coupling employment through the BOX/substrate interface, which modulates the current flow at channel is expected to enhance the detection of cTnI in the sub-threshold area. Hence, in this study, we had characterized the morphological, structural, and electrical properties of the thin film as biocompatibility nanomaterial for integration with biosensor device. The surface functionalization of the thin film was also validated to ensure the thin film's surface is chemically bound with the APTES and GA, as chemical linker for the immobilization of MAb-cTnI as bio-receptor to capture cTnI biomarker with high specificity. In addition, to study the electrical behaviour of the FET biosensor integrated with ZnO-NPs thin film and the effect of substrate-gate coupling, we also had characterized the device by semiconductor parametric analyser. To support our explanation and to validate the electrical characteristic of the fabricated biosensor, a 2D cross sectional structure of the biosensor was also simulated to investigate the effect on the electrical characteristic of the device when 1) V_{SG} was biased at the substrate and 2) interface charges i.e. positive and negative, as representation of biomolecules was introduced on the channel. Further, to explain the ZnO-FET biosensor's ability for bio-sensing application via electrical label-free method, we had demonstrated the device by dropping difference cTnI biomarker concentrations and measured changes in I_D.

3.1. ZnO-NPs thin film characterization

3.1.1. Surface morphology

Fig. 2 shows 2D AFM images of the ZnO-NPs thin film deposited layers. Three various layers were deposited (1, 3, and 5 layers) via spin coating technique in order to analyse their effect on the surface morphology of the thin film. The increase number of deposited layers mostly contributes the thickness increase of the thin films. Based on the measurement obtained from the stylus profilometer,

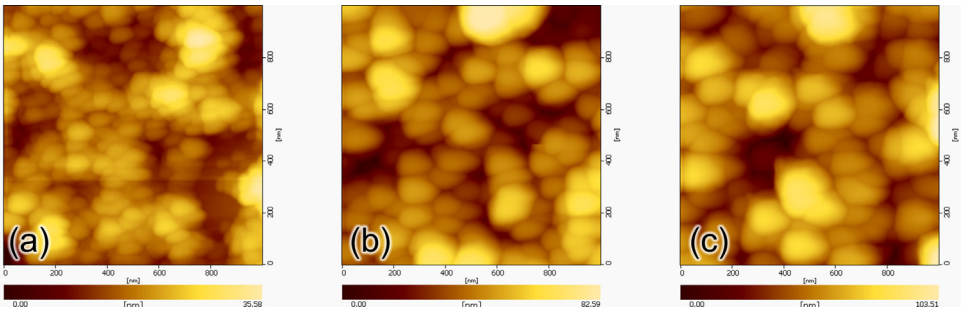

Fig. 2. 2D AFM characterization of ZnO-NPs thin films with different number of deposited layers via sol-gel and spin coating techniques. (a) 1, (b) 3, and (c) 5 deposited layers.

Table 1
ZnO-NPs thin films surface morphology characterization using stylus profilometer and AFM.

Number of deposited layers	Thickness (nm)	Grain size (nm)	Surface roughness, R_a (nm)	MS (nm)
1	80.4	81.61	4.25	5.32
3	206.7	112.79	10.38	13.69
5	353.2	114.58	12.85	16.50

the thicknesses were linearly increased (80.4 nm to 353.2 nm) as the number of deposited layers increased. Additional AFM images in 3D view of the 1, 3, and 5 deposited layers of the thin film as shown in supplementary Fig. S1. The grain sizes of the thin films increased from 81.61 to 114.58 nm when number of deposited layers of the thin film were increased from 1 to 5 deposition layers, hence produced denser thin film [26]. The surface roughnesses of the thin films also showed significant increment with R_a and RMS roughness increase from 4.25 to 12.85 nm and from 5.322 to 16.5 nm, respectively, which occurred due to the thin film become denser, which also related to the increase of grain size, from repetitive deposited layers [26]. The surface roughness for 5 deposited layers is too high, indicating low quality of the thin film, which would cause non-specific adsorption of biomolecules, thus not preferable to be used in bio-sensing application. The result of thickness, grain size, and surface roughness of the thin films were tabulated in Table 1.

Fig. 3 displayed the effects of different ZnO-NPs thin film deposited layers via FESEM images. The thin film appeared denser as the number of deposited layers increased due to grain size of the thin film increased as previously demonstrated from the AFM images. The thin film also appeared less uniform as the number of deposited layers increased due to the increased number of ZnO-NPs on the surface of the thin film.

3.1.2. Structural and crystalline phase

XRD was performed to study the structural and crystalline phase of the ZnO-NPs thin films prepared based on sol-gel and spin coating techniques. The thin films contained matching reflection peaks of (100), (002), (101), and (102) at 2θ are 31.773°, 34.441°, 36.262°, and 47.558°, respectively, which represent the hexagonal wurtzite phase of ZnO (PDF 01-071-6424) [27] (Fig. 4). The surface of the thin films is suitable to be used for biomolecules interaction as the crystallize structure is the most stable at ambient condition [28]. The thin films also exhibited partial orientation of ZnO grains along the desired c-axis, in which the orientation is perpendicular to the surface [29], represented by greater (002) peaks compared to the reference peak. In addition, improvement of the thin film crystallinity can be observed by referring to the increase in reflection peak of the thin film as the deposited layers increased [29].

3.1.3. Electrical characterization

Fig. 5 shows the electrical characteristics for different thicknesses of deposited ZnO-NPs thin film layers, for voltage (V) as a function of current (I). Two Al electrodes (representing source and drain) with dimension of 2 × 2 mm and separated by distance of 10 mm, are deposited on the thin film. Current flows for different deposited layers have been electrically characterized by using SPA at room temperature. A linear response was observed from the V against I curve (Fig. 5(a)), shows the thin films behave like ohmic contact. From Fig. 5(a), the linear response slope of the V against I can be extracted, which represents the resistances (R) for the ZnO NPs thin films. The R of the deposited ZnO-NPs thin films layers are plotted as in Fig. 5(b). The highest resistance is 72.41 MΩ was given by the 1 deposited layer of ZnO-NPs thin film, while thin film with 5 deposited layers was shown to have the lowest R value, i.e., 26.22 MΩ. This implied that with the addition of deposited layers (which increased the thin film thickness), decrease the R of the thin film (Fig. 5(b)), which is in agreement with Eq. (1)

$$R = rho(L/(Wt)) \quad (1)$$

where rho, L, W, and t is the electrical resistivity, length, width, and thickness of the thin film, respectively. This decrease in R is related to the number of deposited layers that had increased the thin film thickness linearly, thus producing denser thin film, which have larger grain size. This is finally contributed to increase of electrical conductance of the thin film, similar to previous report [26].

3.2. Surface functionalization characterization

The functional groups appeared on the ZnO-NPs thin films were examined by using FT-IR spectroscopy (Fig. 6). Fig. 6(a) shows the FT-IR absorption spectra of the ZnO thin film deposited on SiO_2/Si wafer for three consecutive surface functionalization processes, started with functionalization of the thin film with APTES (Fig. 6(b)), GA (Fig. 6(c)), and immobilization of MAb-cTnI (Fig. 6(d)) as bio-receptor for cTnI biomarker. The first step, where a thin and stable layer of APTES, which contains amino (NH_2) group was functionalized to the surface of ZnO-NPs thin film. In Fig. 6(b), two medium peaks at 3383 and 3290 cm^{-1} of N—H stretch vibration with N—H bending vibration peak at 1571 cm^{-1} was noticeable on the FT-IR spectra represent the free NH_2 group of bonded APTES on the ZnO-NPs thin film. In addition, strong peak at 1217 cm^{-1} of C—N stretch and Si—C rock at 828 cm^{-1} from the APTES are available on the thin film. These results suggested APTES is functionalized on the surface of the thin film. GA was the next step, which act as a homobifunctional cross linker with aldehyde groups on both ends with carbon chain spacer [30]. One of GA's end, an aldehyde group binds to the NH_2 group of the APTES layer and produced secondary amide bond, while at the other GA's end, another aldehyde group is free and exposed for immobilization with NH_2 groups of the MAb-cTnI antibodies [31]. The FT-IR spectra after functionalization

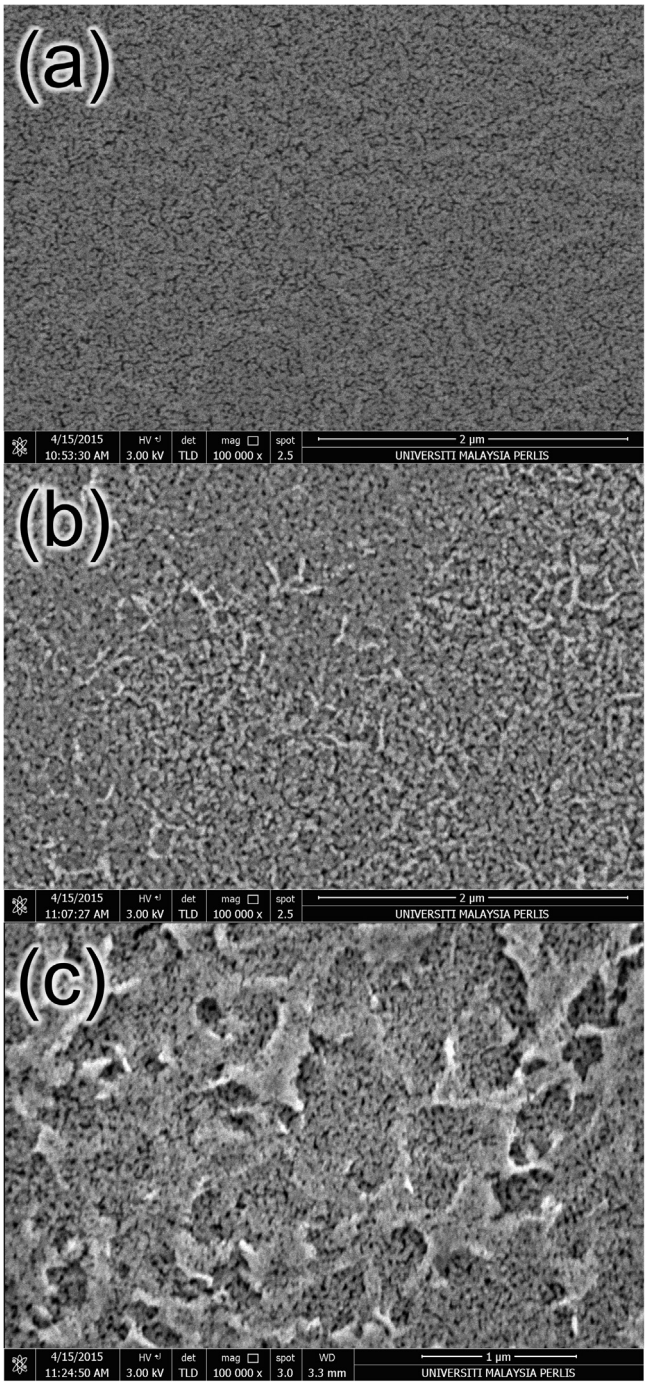

Fig. 3. FESEM images of ZnO-NPs thin films with different number of deposited layers via sol-gel and spin coating techniques. (a) 1, (b) 3, and (c) 5 deposited layers.

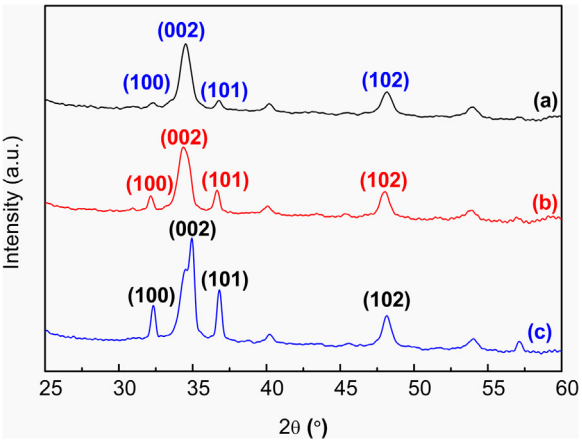

Fig. 4. XRD analysis ZnO-NPs thin films with different number of deposited layers via sol-gel and spin coating techniques. (a) 1, (b) 3, and (c) 5 deposited layers.

with GA (Fig. 6(c)) also presented a strong peak of NH deformation in secondary amides at 1502 cm^{-1},which represents covalent binding between NH_2 group of APTES and aldehyde group of GA. While weak peak of —CHO bending in aldehydes at 2695 cm^{-1} and a strong peak C=O stretch in aldehydes at 1702 cm^{-1} represent the GA's end with free aldehyde group, which can be observed in the FT-IR spectra. The bands associated to the stretching of C—C, C—N, and C—O groups were noticeable in the range 1200–1500 cm^{-1}, while the establishment of amide bond between APTES and GA was observable at peak within the range of 1600–1900 cm^{-1} [31], thus indicates the presence of GA bound to the APTES on the thin film. The NH_2 group of the MAb-cTnI finally immobilized via covalent binding at the aldehyde group of the GA on the surface of the ZnO-NPs thin film, hence forming an amide bond [31]. After immobilization of MAb-cTnI on the GA (Fig. 6(d)), it can be observed that strong peaks of amide stretching at 3735 and 3625 cm^{-1} on the FT-IR spectra from the covalent binding between NH_2 group of the MAb-cTnI to the aldehyde group of GA, while medium peak of C=O in primary amide stretching at 1640 cm^{-1}, which is in agreement with previous report [32]. Other significant bands were observed at 1553 cm^{-1} resulted by N—H deformation in secondary amide, and strong peak at 1669 cm^{-1} resulted by C=O from carboxylic acids stretching, which are available on the MAb-cTnI. The surface functionalization processes of the ZnO-NPs thin film are represented as in Fig. 6(e) to give a clear view of the functional groups available at each surface functionalization stages. All FT-IR spectras in Fig. 6 contained a band corresponding to gas-phase CO_2 between ~2300 to 2400 cm^{-1}, indicating the measurements were exposed to a CO_2 atmosphere [33]. Fig. 6(e) illustrated the overall stages of the surface functionalization on the thin film.

3.3. *Effect on electrical characteristic of substrate-gate on ZnO-FET biosensor*

Fig. 7(a) shows the electrical characterization of (i) fabricated and (ii) simulated ZnO-FET biosensors, respectively, as a function of I_D with various V_{SG} (V_{SG} = −2, −1, 0, 1, and 2 V) performed at room temperature. The fabricated ZnO-FET biosensor with substrate-gate coupling utilized 3 deposited layers of ZnO-NPs thin film, instead of 1 deposited layer in order to produce thicker thin film [34], with good surface roughness, high uniformity, and moderate resistance based on AFM, FESEM, and electrical characterization results as in previous discussion (Figs. 2, 4 and 5). The electrical characterization is shown in Fig. 7(a)(i) (experimental) and Fig. 7(a)(ii) (simulation). Both results show very good correlation between fabrication (Fig. 7(a)(i)) and simulation (Fig. 7(a)(ii)), where both exhibit a linear characteristic during forward biased, and shift of V_T to the left with increases of I_D for negatively V_{SG}. Opposite trend can be observed for positively V_{SG}. Very good agreement between simulated and fabricated result is justified for further analysis, to explain the electron concentration behaviour as a function of V_{SG}. The difference in terms of value between experimental and simulation was contributed by several factors, i.e., 1) we assumed the doping concentration of ZnO-NPs thin film is 10^{15} cm^{-3} during device simulation modelling to represent ZnO-NPs thin film material used in the fabricated biosensor, 2) the default mobility value available in the software was used to compensate the unknown mobility values of deposited ZnO-NPs thin

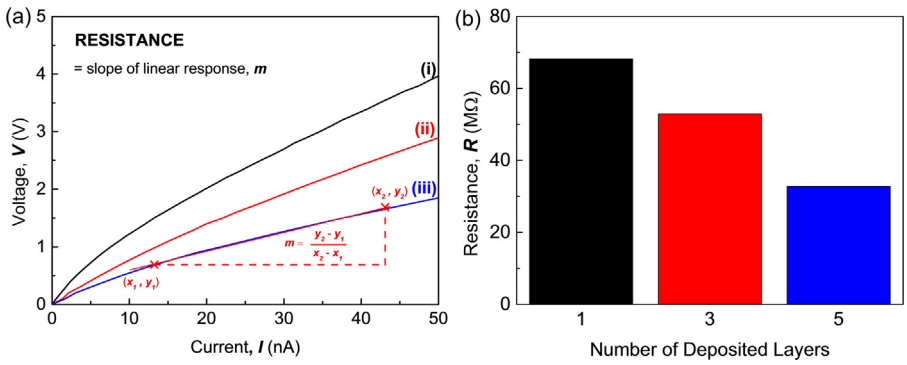

Fig. 5. Electrical characterization of ZnO-NPs thin films with different number of deposited layers via sol-gel and spin coating techniques. (a) V against I characteristic of (i) 1, (ii) 3, and (iii) 5 deposited layers. (b) Resistance histogram of the deposited thin film layers.

film, 3) the device modelling simulation utilized ZnO thin film as a bulk material, while the deposited ZnO is based on agglomeration of ZnO nanoparticles to form the ZnO-NPs thin film via sol-gel technique. Although the produced results were disparate in terms of value, the trend from the experimental resembles the trend of the simulation. Shift in current trend is translated into changes in V_T and I_D, which will be discussed next.

Different V_{SG} bias effect on the simulated 2D FET structure was further investigated on the electron concentration at specific coordinate. Fig. 7(b) shows the horizontal cut near (i) the buried oxide/substrate interface and (ii) near the surface of *p*-*n*-p junction. As shown in electron concentration cut in Fig. 7(b)(i), at negatively V_{SG} bias ($V_{SG} = -1$ and -2 V), accumulation of high electron concentration, thus introducing the inversion space charge condition in the p-type Si substrate along the BOX/Si substrate interface. This result causes the accumulation of holes, producing a hole conduction layer along the source, gate, and drain region (Fig. 7(b)(ii)), and allows more current flow between source and drain. This concept is the same with theoretical metal-oxide semiconductor FET (MOSFET) operation, whereby to enable high current flow through *p*-*n*-p junction, formation of a hole conduction layer in the n-type region is required. Thus, its explained why the increase of I_D and at the same time, due to shift in V_T toward lower V_D. We would like to stress out, although ZnO is n-type material, however the characteristic is changed due to 1) the presence of *p*-*n*-p junction between source, channel and drain, and 2) the voltage biasing from the substrate-gate coupling. Both conditions play an important role to change the characteristic of ZnO material deposited at the channel. On the contrary, as positively V_{SG} bias ($V_{SG} = 1$ and 2 V) are given to the substrate-gate electrode, the electron concentration along the BOX/Si substrate interface has become lesser, especially at the location beneath the source region, hence reduced the hole concentration inside hole conduction layer at the gate region. This has resulted in reduction of I_D, simultaneously shifting of V_T to higher V_D as positively V_{SG} bias was applied to the substrate-gate voltage.

Fig. 7(c) further illustrated the effect of electron concentration behaviour on the I_D against V_D characteristic obtained from fabricated device. We extracted the V_Ts from linear interpolation of the I_D in linear region as illustrated in Fig. 7(c), similar to the definition for *p*-*n* junction device. When $V_{SG} = 0$ V was supplied to the substrate-gate electrode (Fig. 7(c)(i)), V_T for the device appeared to be at 2.51 V. However, when the V_{SG} were negatively bias ($V_{SG} = -1$ and -2 V) (Fig. 7(c)(ii)), the V_Ts were shifting toward lower voltage value, i.e., 0.64 V and 1.61 V, respectively. In contrast, as positively bias of V_{SG} from 1 to 2 V were supplied to the substrate, the V_Ts were shifted to 3.52 V and 4.50 V respectively (Fig. 7(c)(iii)). As mentioned previously, the production of hole conduction layer by accumulation of high hole concentration in the n-type ZnO-NPs thin film during negatively bias of V_{SG}, due to inversion space charge condition at the BOX/Si substrate has influences the shifting of V_T toward lower V_D. While depending on the V_{SG} value, negatively or positively bias has shifts the V_T toward lower or higher V_D, respectively. Hence, the lower or higher V_T contributes to the increase or decrease of I_D. Table 2 tabulated V_T and I_D for various V_{SG} applied to the fabricated ZnO-FET biosensor.

Table 2
Changes of V_T and I_D of fabricated ZnO-FET biosensor when biased with various V_{SG}.

V_{SG} (V)	V_T (V)	I_D at $V_D = 5$ V (μA)
−2	0.64	15.53
−1	1.61	11.14
0	2.51	7.33
1	3.52	4.29
2	4.50	1.25

3.4. Detection of cardiac troponin I

A device modelling of the 2D cross-sectional structure was performed to investigate the effect of extra charges, introduced on the surface of the channel region. These extra charges function as representation of charged target biomolecules after being captured on the channel's surface. Their effect on electrical characteristic of the simulated device are illustrated in Fig. 8. Application of negatively interface charge density (Q_F) ($Q_F = -6 \times 10^{10}$ cm^{-2}), as negatively charged target biomolecules while biasing the substrate-gate electrode ($V_{SG} = -2$ V) on the simulated 2D cross sectional structure, have attracted hole carrier inside the ZnO channel region due to opposite charges and increased the hole concentration, further produced an enhanced hole conduction layer (which is previously clarified in section 3.3) between the p-type source and drain (Fig. 8(a)), allowing more current flow. This explained the increase in value of I_D observed in Fig. 8(b). In contrast, decrease in I_D values were observed (Fig. 8(b)) when positively Q_F, acts as positively charged target biomolecules was introduced on the surface of the channel ($Q_F = 6 \times 10^{10}$ cm^{-2}). Based on Fig. 8(a), the hole concentration at the channel decreased significantly due to repulsive force by the same positively charge, present on the channel surface, hence diminished the hole conduction layer between the p-type source and drain (Fig. 8(a)), and reducing current flow. These results give us a clear indication in order to understand the electrical characteristic of ZnO-FET biosensor with substrate-gate coupling when used for detection of positively or negatively charges target biomolecules.

The simulated results in Fig. 8(b) correlated well with the fabricated biosensor, which also resembled the same electrical characteristic when cTnI biomarker bound to the MAb-cTnI on the channel's surface (Fig. 9(a)). Based on previous discussion, we have chosen $V_{SG} = -2$ V for the cTnI biomarker detection, since better modulation at of V_{SG}, translated into higher current at $V_D = 1$ V.

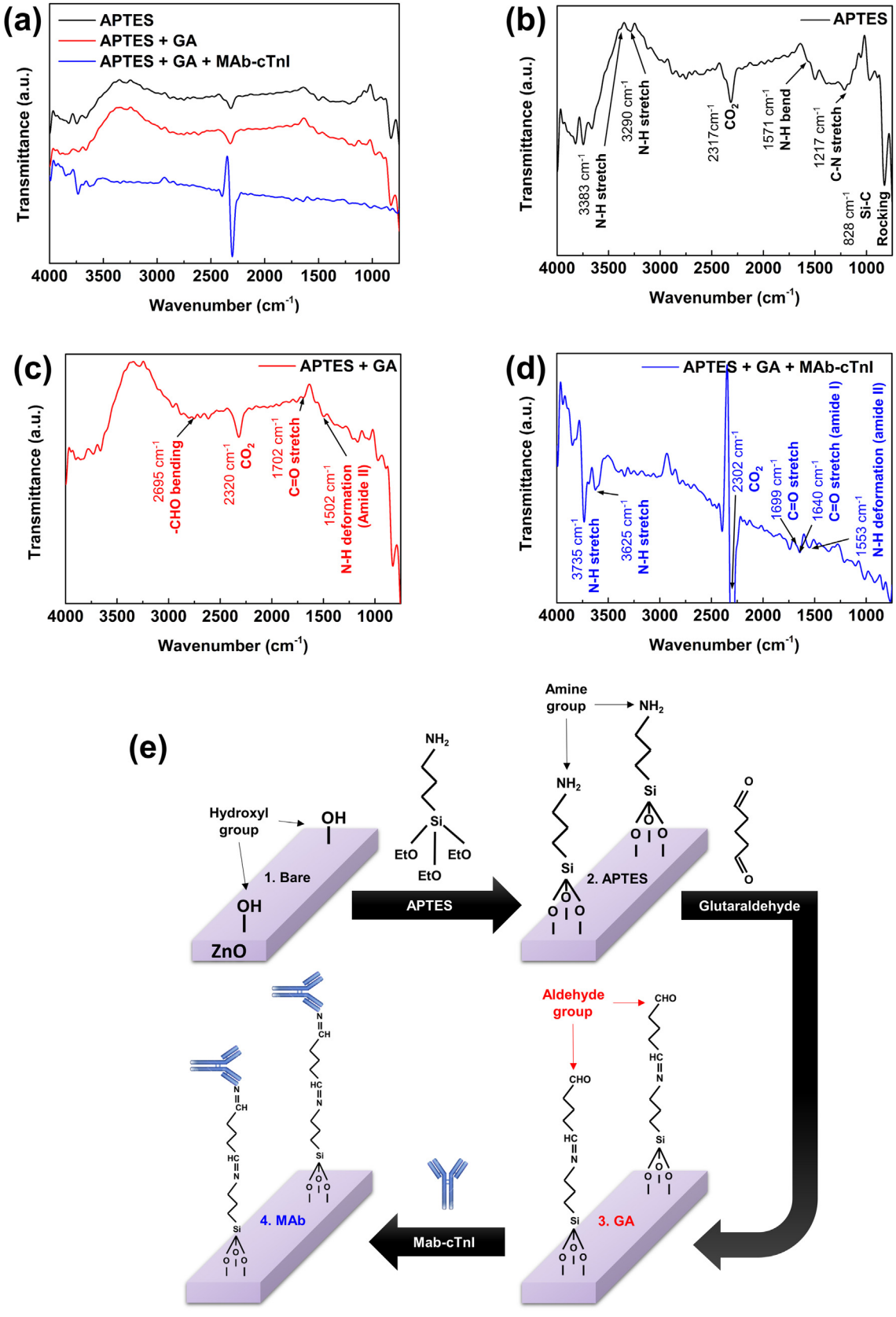

Fig. 6. Surface functionalization characterization of ZnO-NPs thin film. (a) FT-IR spectra adsorption of ZnO-NPs thin film deposited with (b) APTES, (c) GA, and (d) MAb-cTnI to functionalize the surface for capturing cTnI biomarker. (e) Overall stages of the surface functionalization on the thin film.

Table 3
Comparison of available FET-based biosensors for cTnI biomarker detection with their specifications.

FET-based Method	Surface Functionalization	Linkers	Bio-receptor	Sample volume (μL)	LOD (pg/mL)	Advantages	Reference
Silicon Nanowire							
CMOS SINWs FET	Covalent binding	1% APTES + 2.5% GA	MAb cTnI	50	92.0	High sensitivity, selective, mass-producible, and anti-interference.	[35]
High-k/oxide stacked dielectric structure multi-channel SINW	Covalent binding	2% APTES + 2.5% GA	Ab-cTnI	~5	~7.6	Better sensing performance.	[22]
Honeycomb SINW FETs	Covalent binding	1% APTES + 5% GA	MAb-cTnI	1	~5.0	High sensitivity, high selectivity, increased sensing area	[24]
Conducting Polymer Nanowire							
Single PANI nanowire	Covalent binding	EDC + NHS	MAb-cTnI, MAb-Myo, MAb-CK-MB, MAb-CK-MM	~60	0.3	Ultra-sensitivity, good sensing reproducibility, and high selectivity.	[36]
Carbon-based Materials							
SWNTs/GNPs hybrid FET	Covalent binding	PyMe-NH2 + MPA/GNPs	Ab-cTnI	~1	1.0	Ultra-sensitivity, high selectivity, and label-free	[37]
Graphene-gated biochip	Covalent binding	EDC + NHS	MAb-cTnI	~10	0.1	Highly sensitive and label-free.	[25]
Bio-functionalized f-RG FET	Covalent binding	None	Anti-cTnI	~1	1.0	High sensitivity and selectivity; label-free, require no additional bilinkers.	[38]
Tin Oxide Nanobelt							
Functionalized SnO2 nanobelt FETs	Covalent binding	APTES + biotin + Streptavidin + biotin	Anti-cTnI	n/a	~2000.0	Real-time and high selectivity.	[39]
Zinc Oxide Nanoparticles							
ZnO-NPs thin film FET with Substrate-gate coupling	Covalent binding	2% APTES + 2.5% GA	MAb-cTnI	1	3.24	High sensitivity, high selectivity, low cost deposition technique, low complexity fabrication process.	This work

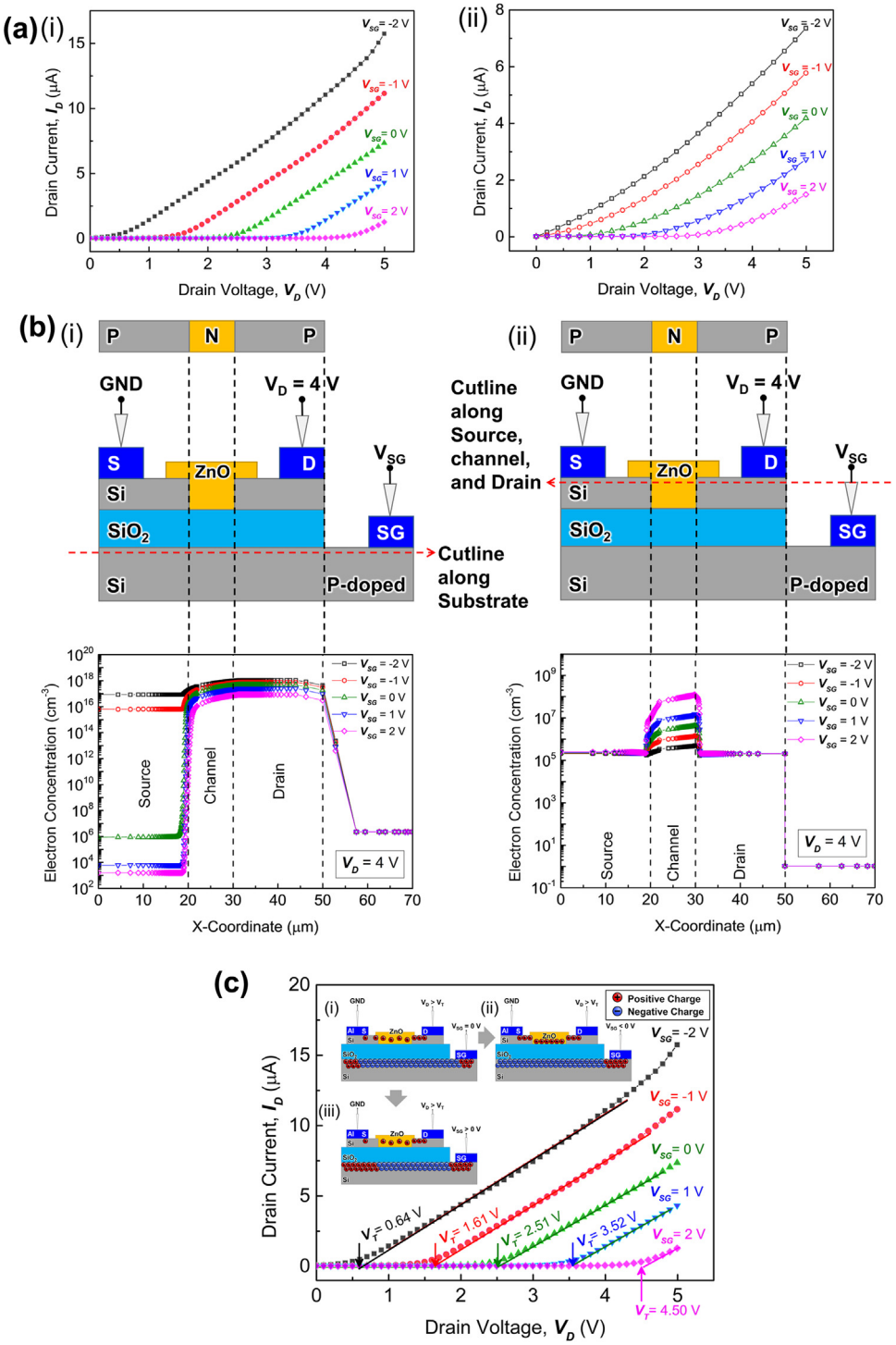

Fig. 7. Different V_{SG} bias effect on the ZnO-FET biosensor with substrate-gate coupling. (a) Comparison in term of I_D against V_D characteristic between (i) fabricated and (ii) simulated device. (b) Electron concentration along the cutline of the simulated 2D FET structure at (i) BOX/Si substrate interface, underneath the source, gate, and drain region; (ii) near the surface of the source, gate and drain region. (c) Shifting of V_T and I_D due to (i) without, (ii) negatively, and (iii) positively bias of V_{SG}.

The device exhibited a significant decrease in measured I_D as the concentrations of cTnI biomarker were increased from 1 ng/ml, 10 ng/ml, 100 ng/ml, 1 ug/ml to 10 ug/ml. This event occurs due to the fact that cTnI biomarkers have high positive charge (pI 9.87) [20], which repulse the positively charge, decreased the hole concentration, and thus diminished the hole conduction layer (which was formed at the channel after application of negatively V_{SG} to the substrate, as explained previously in Section 3.3) of the ZnO-NPs thin film between p-type source and drain region, hence reduced the measured I_D. The calibration curve slope in Fig. 9(b) obtained from linear response of I_D with the increase cTnI biomarker concentration from 1 ng/ml to 10 μg/ml, represented the sensitivity of our biosensor [9], which is 35.3 nA (g/ml)$^{-1}$. Furthermore, the biosensor's ability to identify the lowest concentration, which is the limit of detection (LOD) of cTnI biomarker was analysed as in Fig. 9(c). The biosensor produced a linear response of relative change in the

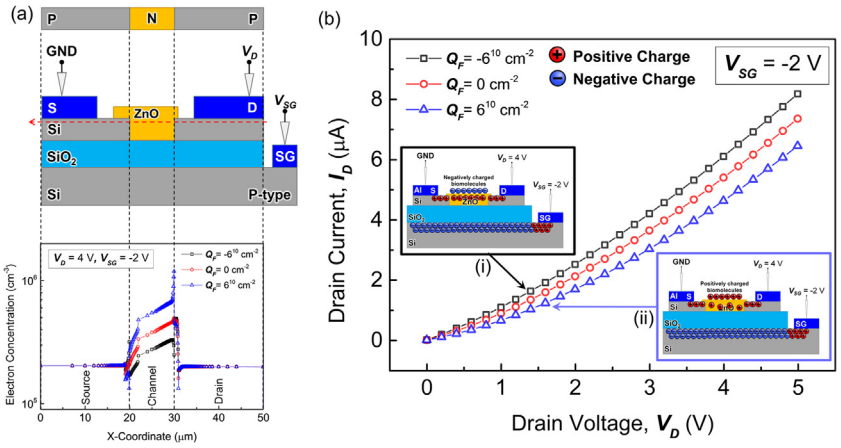

Fig. 8. Effect of extra charges introduced at the surface of the ZnO-NPs thin film as channel of the ZnO-FET biosensor with substrate-gate coupling. (a) Electron concentration along the cutline of the simulated 2D FET structure near the surface of the source, gate and drain region. (b) I_D against V_D characteristic of the biosensor with introduction of (i) negative and (ii) positive Q_F.

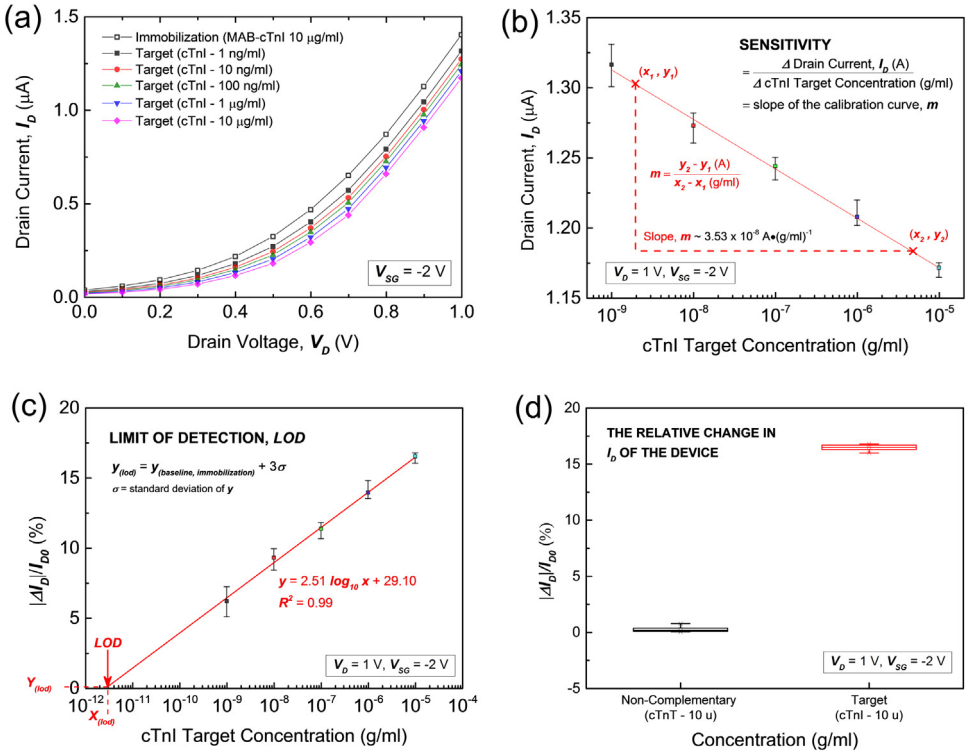

Fig. 9. Detection of cTnI target biomarker at different concentrations (1 ng/ml to 10 μg/ml) using the ZnO-FET biosensor at sweep V_D of 0–1 V with V_{SG} = −2 V. (a) I_D against V_D characteristic at different cTnI biomarker concentrations. (b) I_D response curve of the biosensor with substrate-gate coupling at different cTnI target biomarker concentrations. (c) Calibration curve of the relative change in I_D, shows the LOD. (d) The relative change of I_D for 10 μg/ml cTnT (non-complementary protein as control) and 10 μg/ml of cTnI target biomarker.

measured I_D over the logarithmic cTnI biomarker concentration ranging from 1 ng/ml to 10 μg/ml with LOD of 3.24 pg/ml based on calculation from the standard deviation of the response and the calibration curve's slope [9]. The calculation to determine the LOD of our biosensor is included in supplementary explanation E1. The specificity of the biosensor was also confirmed by quantifying and comparing the biosensor's relative change of I_D based on plotted box chart, before and after protein binding of the channel surface with 10 μg/ml of cTnT biomarker as non-specific protein (control), and 10 μg/ml of cTnI target biomarker (Fig. 9(d)). In comparison, a significant change in I_D (~17%) was displayed by 10 μg/ml of cTnI biomarker compared to 10 μg/ml cTnT non-complementary biomarker (~1%). Only cTnI biomarker, which exhibited a specific binding to the immobilized MAb-cTnI as bio-receptor allows the relative changes in measured I_D. To evaluate the precision and repeatability of the biosensor, reproducibility of FET biosensor by comparing five different devices was conducted as in supplementary Fig. S2. The result demonstrated an acceptable reproducibility performance of the biosensor with RSD was calculated at ~19%. The high RSD might be due to the agglomeration of ZnO-NP to form the ZnO-NPs thin film, which produced uneven surface when compared to another device, thus contributed to the minor variation in the result. Comparison of our device's performance with the previously published is tabulated in Table 3.

4. Conclusion

The present study on ZnO-NPs thin film with its characterization in terms of surface morphology, crystalline phase, electrical conductivity, and surface functionalization capability has been explained and concluded with accomplished integration of substrate-gate and FET-based biosensor. Integration of the n-type ZnO-NPs thin film at the micro-sized channel between two p-type top-silicon layer, has created the *p-n*-p junction between source, channel, and drain, respectively, developing a device capable for bio-sensing application. With the presence of V_{SG} biasing, the modulation of the channel can be achieved, which shows changes in V_T with difference value of I_D. The mechanism of the changes in V_T and I_D due to V_{SG} bias has been explained with the aid of simulation, through the electron concentration characteristics, and the results are correlated well with the fabricated biosensor. The negatively biased of V_{SG}, which formed hole conduction layer at lower V_D range (at V_D = 1 V) causes decrease of the V_T (0.65 V), thus allow more I_D to flow across the channel between p-type source to drain region. Upon detection of high positive charge of cTnI biomarker, the I_D in the channel decreases, signifying detection of the biomolecule. Therefore, detection of various cTnI biomarker concentration with high sensitivity was succesfully performed with the biosensor's LOD is down to 3.24 pg/ml. Immobilization of MAb-cTnI through covalent binding on the surface of the ZnO-NPs thin film has allowed detection of cTnI biomarker with high specificity. With unique characteristic and electrical properties offered by ZnO, combine with advantages of substrate-gate coupling in FET biosensor for the detection of target biomolecules will surely open up a new path towards future innovative developments of FET biosensor utilizing more advance nanomaterial.

Conflict of interest

The authors declare no competing financial interest.

Acknowledgments

The authors are grateful to the Department of Higher Education, Ministry of Higher Education (KPT), for funding this research through the Fundamental Research Grant Scheme (FRGS; with the Grant number 9003-00536). The authors also would like to acknowledge all the team members in Institute of Nano Electronic Engineering (INEE), Universiti Malaysia Perlis (UniMAP) for their guidance and help.

Appendix A. Supplementary data

Supplementary data associated with this article can be found, in the online version, at http://dx.doi.org/10.1016/j.snb.2016.09.131.

References

[1] D. Sarkar, W. Liu, X. Xie, A.C. Anselmo, S. Mitragotri, K. Banerjee, MoS 2 field-Effect transistor for next-generation label-Free biosensors, ACS Nano 8 (2014) 3992–4003.
[2] S. Liu, X. Guo, Carbon nanomaterials field-effect-transistor-based biosensors, NPG Asia Mater. 4 (2012) e23–10.
[3] E. Buitrago, M.F.-B. Badia, Y.M. Georgiev, R. Yu, O. Lotty, J.D. Holmes, A.M. Nightingale, H.M. Guerin, A.M. Ionescu, Electrical characterization of high performance, liquid gated vertically stacked SiNW-based 3D FET biosensors, Sens. Actuators B Chem. 199 (2014) 291–300.
[4] P. Dai, A. Gao, N. Lu, T. Li, Y. Wang, A back-gate controlled silicon nanowire sensor with sensitivity improvement for DNA and pH detection, Jpn. J. Appl. Phys. 52 (2013) 121301.
[5] Z. Iskierko, M. Sosnowska, P.S. Sharma, T. Benincori, F. D'souza, I. Kaminska, K. Fronc, K. Noworyta, Extended-gate field-effect transistor (EG-FET) with molecularly imprinted polymer (MIP) film for selective inosine determination, Biosens. Bioelectron. 74 (2015) 526–533.
[6] J. Lee, J. Jang, B. Choi, J. Yoon, J.-Y. Kim, Y.-K. Choi, D. Myong Kim, D. Hwan Kim, S.-J. Choi, A highly responsive silicon nanowire/amplifier MOSFET hybrid biosensor, Sci. Rep. 5 (2015) 12286.
[7] J. Li, M. Sun, X. Wei, L. Zhang, Y. Zhang, An electrochemical aptamer biosensor based on gate-controlled effect using β-cyclodextrin for ultra-sensitive detection of trace mercury, Biosens. Bioelectron. 74 (2015) 423–426.
[8] J.-K. Park, H.-J. Jang, J.-T. Park, W.-J. Cho, SOI dual-gate ISFET with variable oxide capacitance and channel thickness, Solid. State. Electron. 97 (2014) 2–7.
[9] M. Nuzaihan M.N, U. Hashim, M.K. Md Arshad, S.R. Kasjoo, S.F.A. Rahman, A.R. Ruslinda, M.F.M. Fathil, R. Adzhri, M.M. Shahimin, Electrical detection of dengue virus (DENV) DNA oligomer using silicon nanowire biosensor with novel molecular gate control, Biosens. Bioelectron. 83 (2016) 106–114.
[10] J.-H. Ahn, S.-J. Choi, J.-W. Han, T.J. Park, S.Y. Lee, Y.-K. Choi, Double-gate nanowire field effect transistor for a biosensor, Nano Lett. 10 (2010) 2934–2938.
[11] P.G. Fernandes, R.A. Chapman, O. Seitz, H.J. Stiegler, H.-C. Wen, Y.J. Chabal, E.M. Vogel, Effect of back-gate biasing on floating electrolytes in silicon-on-Insulator-Based nanoribbon sensors, IEEE Electron Device Lett. 33 (2012) 447–449.
[12] S.P. Singh, S.K. Arya, P. Pandey, B.D. Malhotra, S. Saha, K. Sreenivas, V. Gupta, Cholesterol biosensor based on rf sputtered zinc oxide nanoporous thin film, Appl. Phys. Lett. 91 (2007) 063901.
[13] Q. Xu, C. Mao, N.-N. Liu, J.-J. Zhu, J. Sheng, Direct electrochemistry of horseradish peroxidase based on biocompatible carboxymethyl chitosan–gold nanoparticle nanocomposite, Biosens. Bioelectron. 22 (2006) 768–773.
[14] X. Zhu, I. Yuri, X. Gan, I. Suzuki, G. Li, Electrochemical study of the effect of nano-zinc oxide on microperoxidase and its application to more sensitive hydrogen peroxide biosensor preparation, Biosens. Bioelectron. 22 (2007) 1600–1604.
[15] S. Kumar, V. Gupta, K. Sreenivas, Synthesis of photoconducting ZnO nano-needles using an unbalanced magnetron sputtered ZnO/Zn/ZnO multilayer structure, Nanotechnology 16 (2005) 1167–1171.
[16] J.X. Wang, X.W. Sun, A. Wei, Y. Lei, X.P. Cai, C.M. Li, Z.L. Dong, Zinc oxide nanocomb biosensor for glucose detection, Appl. Phys. Lett. 88 (2006) 233106.
[17] Y. Zhang, Z. Kang, X. Yan, Q. Liao, ZnO nanostructures in enzyme biosensors, Sci. China Mater. 58 (2015) 60–76.
[18] X. Liu, P. Lin, X. Yan, Z. Kang, Y. Zhao, Y. Lei, C. Li, H. Du, Y. Zhang, Enzyme-coated single ZnO nanowire FET biosensor for detection of uric acid, Sens. Actuators B Chem. 176 (2013) 22–27.
[19] K. Ogata, H. Dobashi, K. Koike, S. Sasa, M. Inoue, M. Yano, Patterned growth of ZnO nanorods and enzyme immobilization toward the fabrication of glucose sensors, Phys. E Low-Dimensional Syst. Nanostructures. 42 (2010) 2880–2883.
[20] S. Eriksson, Negative interference in cardiac troponin I immunoassays from a frequently occurring serum and plasma component, Clin. Chem. 49 (2003) 1095–1104.
[21] Y.W. Heo, S.J. Pearton, D.P. Norton, F. Ren, Chapter 5. ZnO thin-Film and nanowire-based sensor applications, in: Semicond Device-Based Sensors Gas, Chem. Biomed. Appl, CRC Press, 2011, pp. 149–214.
[22] S.-H. Shen, I.-S. Wang, H. Cheng, C.-T. Lin, An enhancement of high-k/oxide stacked dielectric structure for silicon-based multi-nanowire biosensor in cardiac troponin I detection, Sens. Actuators B Chem. 218 (2015) 303–309.
[23] J.H. Chua, R. Chee, A. Agarwal, S.M. Wong, G. Zhang, Label-free electrical detection of cardiac biomarker with complementary metal-Oxide semiconductor-compatible silicon nanowire sensor arrays, Anal. Chem. 81 (2009) 6266–6271.
[24] K. Kim, C. Park, D. Kwon, D. Kim, M. Meyyappan, S. Jeon, J.-S. Lee, Silicon nanowire biosensors for detection of cardiac troponin I (cTnI) with high sensitivity, Biosens. Bioelectron. 77 (2016) 695–701.
[25] S.K. Tuteja, Priyanka, V. Bhalla, A. Deep, A.K. Paul, C.R. Suri, Graphene-gated biochip for the detection of cardiac marker Troponin I, Anal. Chim. Acta. 809 (2014) 148–154.
[26] H. Youl Bae, Electrical and reducing gas sensing properties of ZnO and ZnOCuO thin films fabricated by spin coating method, Sens. Actuators B Chem. 55 (1999) 47–54.
[27] T. Sahoo, M. Kim, M.-H. Lee, L.-W. Jang, J.-W. Jeon, J.S. Kwak, I.-Y. Ko, I.-H. Lee, Nanocrystalline ZnO thin films by spin coating-pyrolysis method, J. Alloys Compd. 491 (2010) 308–313.
[28] J.L.G. Fierro, Metal Oxides: Chemistry and Applications, CRC Press, 2005.
[29] A.A. Mosquera, D. Horwat, A. Rashkovskiy, A. Kovalev, P. Miska, D. Wainstein, J.M. Albella, J.L. Endrino, Exciton and core-level electron confinement effects in transparent ZnO thin films, Sci. Rep. 3 (2013) 1714.
[30] S.C.B. Gopinath, K. Awazu, M. Fujimaki, K. Shimizu, W. Mizutani, K. Tsukagoshi, Surface functionalization chemistries on highly sensitive silica-based sensor chips, Analyst 137 (2012) 3520.
[31] N.S.K. Gunda, M. Singh, L. Norman, K. Kaur, S.K. Mitra, Optimization and characterization of biomolecule immobilization on silicon substrates using (3-aminopropyl)triethoxysilane (APTES) and glutaraldehyde linker, Appl. Surf. Sci. 305 (2014) 522–530.
[32] R.C. Triulzi, M. Micic, J. Orbulescu, S. Giordani, B. Mueller, R.M. Leblanc, Antibody–gold quantum dot-PAMAM dendrimer complex as an immunoglobulin immunoassay, Analyst 133 (2008) 667.
[33] J. Fujiki, K. Yogo, Carbon dioxide adsorption onto polyethylenimine-functionalized porous chitosan beads, Energy Fuels 28 (2014) 6467–6474.

[34] K.L. Foo, M. Kashif, U. Hashim, M.E. Ali, Fabrication and characterization of ZnO thin films by sol-gel spin coating method for the determination of phosphate buffer Saline concentration, Curr. Nanosci. 9 (2013) 288–292.
[35] T. Kong, R. Su, B. Zhang, Q. Zhang, G. Cheng, CMOS-compatible, label-free silicon-nanowire biosensors to detect cardiac troponin I for acute myocardial infarction diagnosis, Biosens. Bioelectron. 34 (2012) 267–272.
[36] I. Lee, X. Luo, J. Huang, X.T. Cui, M. Yun, Detection of cardiac biomarkers using single polyaniline nanowire-based conductometric biosensors, Biosensors 2 (2012) 205–220.
[37] Rajesh, V. Sharma, N.K. Puri, R.K. Singh, A.M. Biradar, A. Mulchanadani, Label-free detection of cardiac troponin-I using gold nanoparticles functionalized single-walled carbon nanotubes based chemiresistive biosensor, Appl. Phys. Lett. 103 (2013) 203703.
[38] S.K. Tuteja, P. Sabherwal, A. Deep, R. Rastogi, A.K. Paul, C.R. Suri, Biofunctionalized rebar graphene (f-RG) for label-free detection of cardiac marker troponin I, ACS Appl. Mater. Interfaces 6 (2014) 14767–14771.
[39] Y. Cheng, K.-S. Chen, N.L. Meyer, J. Yuan, L.S. Hirst, P.B. Chase, P. Xiong, Functionalized SnO_2 nanobelt field-effect transistor sensors for label-free detection of cardiac troponin, Biosens. Bioelectron. 26 (2011) 4538–4544.

Biographies

Mohamad Faris Bin Mohamad Fathil received his bachelor's degree in Microelectronic Engineering from Universiti Malaysia, Perlis (UniMAP), Malaysia in 2013. He is currently working towards his doctorate degree at Institute of Nano Electronic Engineering (INEE), UniMAP. His research interests are in the area of nanoelectronic engineering and biosensor application. His research work is exploring the fabrication process for zinc oxide field effect transistor (ZnO-FET) and back gate biasing to develop an electrical-based biosensor for cardiac troponin detection.

Ir. Dr. Mohd Khairuddin Md Arshad earned his doctorate degree from Universite Catholique de Louvain (UCL), Belgium in 2013. He is a senior lecturer in Universiti Malaysia Perlis and a deputy director at Institute of Nano Electronic Engineering, and currently working in the field of biosensor, FET, advanced SOI based MOSFET and advanced packaging. Previously, he worked with Agilent Technologies (M) Sdn Bhd, Penang and ON Semiconductor (M) Sdn. Bhd, Negeri Sembilan Malaysia.

Dr. Ruslinda A. Rahim obtained her doctorate degree in 2012 from Waseda University, Japan. She is a senior lecturer in Universiti Malaysia Perlis and a deputy dean for R&D Department. Her interest involves FET biosensor, nanostructure fabrication and carbon based materials.

Dr. Subash C.B. Gopinath earned his doctorate degree from the University of Madras in 1999. The same year, he moved to Taiwan to work in the Institute of Academia Sinica. In 2003, he was awarded as JSPS Fellow and continued to work in National Institute of Advanced Industrial Science and Technology, Japan. In 2015, he moved to Universiti Malaysia Perlis. His interest is in aptamer technology, biosensors and RNA-ligand interactions. In the field of biosensor, he uses BioDVD platform technology, Surface Plasmon Resonance and Evanescent-field coupled waveguide.

Mohammad Nuzaihan Md Nor is working as senior lecturer at INEE, UniMAP. He obtained his M.Sc degree in microelectronic engineering from UniMAP and B.Eng in electronic engineering from UTM in 2002 and 2007, respectively. His current researches project focus on the top-down nano fabrication of silicon nanowires for biomedical application.

Adzhri Rahmat holds a degree in microelectronic engineering from Universiti Malaysia Perlis at 2014. Within the same year, he pursues his study in master of nanoelectronic engineering in the same university. His interest is in microelectronic devices, field-effect transistor and biosensors. Currently, his works is focusing on the application of metal oxide towards the field-effect transistor based biosensors.

Prof. Dr. Uda Hashim is a Senior Professor (VK6-B) in UniMAP. He has 14 years of working experience in the CMOS wafer fabrication foundry before joining Universiti Malaysia Perlis (UniMAP) in February 2002 as a lecturer and principle researcher in the School of Microelectronic Engineering. His currently serve as a Director to The Institute of Nano Electronic Engineering (INEE), UniMAP since 2008 until now. He actively involved in research and development activities especially in the area of microelectronics and nanoelectronics engineering leading to nano biosensor, DNA Chips, Microfluidic and Nano Lab-OnChip devices for medical, food and agriculture applications.